Applied Catalysis B: Environmental 205 (2017) 310–318

Contents lists available at ScienceDirect

Applied Catalysis B: Environmental

journal homepage: www.elsevier.com/locate/apcatb

Tailoring dual redox-acid functionalities in $VO_x/TiO_2/ZSM5$ catalyst for simultaneous abatement of PCDD/Fs and NO_x from municipal solid waste incineration

M. Gallastegi-Villa, A. Aranzabal*, J.A. González-Marcos, J.R. González-Velasco

Group "Chemical Technologies for Environmental Sustainability", Chemical Engineering Dept., Faculty of Sciences and Technology, University of the Basque Country UPV/EHU, P.O. Box 644, E-48080 Bilbao, Spain

ARTICLE INFO

Article history:
Received 27 July 2016
Received in revised form
25 November 2016
Accepted 7 December 2016
Available online 8 December 2016

Keywords:
MSW plants
NO_x
PCDD/Fs
Catalytic removal
VO_x/TiO_2
VO_x/zeolite
Bifunctional catalyst

ABSTRACT

A series of $VO_x/TiO_2/ZSM5$ were prepared in order to enhance the acid functionalities of commercially used VO_x/TiO_2 for the combined abatement of NO and o-dichlorobenzene (o-DCB, model molecule to simulate dioxins and furans) from the off-gases of a Municipal Solid Waste (MSW) incinerator plant. The catalysts have been prepared by wet impregnation varying the TiO_2 content from 0 to 46%. VO_x/TiO_2 was also prepared as a reference sample.

Combining catalysts characterization (N_2 adsorption-desorption isotherms, XRD, TEM, NH_3-TPD, H_2-TPR and Raman) and activity data, we found that high TiO_2 loading $VO_x/TiO_2/ZSM5$ catalyst, is highly suitable catalyst for *dDiNOx* process. The NO conversion is higher than the reference VO_x/TiO_2 catalyst partly due to higher amount of acid sites provided by the zeolite and partly due to Ti-V interaction, which is a key factor in the conversion of both o-DCB and NO. The TiO_2 is heterogeneously dispersed over zeolite, but VO_x dispersion is enhanced as the TiO_2 content is increased, leading to a higher active polymeric species contribution, as in the sample V/46Ti/Z (confirmed by correlation between TOF and Ti-V interaction).

1. Introduction

The environmental laws are becoming more and more restrictive and therefore waste treatment technologies need to be improved accordingly. Incineration of Municipal Solid Waste (MSW) has been practiced for many years in western countries since it is the most efficient way to reduce the waste volume (about 90%) and demand for landfill space. However this practice is strongly questioned since harmful pollutants (fly ash, acid gases, NO_x, dioxins and furans, etc.) may be emitted into the air, land and water which is detrimental to human health and environment, in the absence of effective controls. Although incineration of MSW coupled with energy recovery can form an essential part of an integrated waste management system [1], yet strict controls are required to prevent its negative impacts on human health and environment. In this regard, growing number of MSW incineration plants have moved to the more efficient Selective Catalytic Reduction (SCR) with ammonia to abate NO_x emissions. The most common commercial catalyst is V_2O_5–WO_3 (MoO_3)–TiO_2 [2] and some catalyst manufacturers claimed that this catalyst is able to simultaneously destroy dioxin/furans (PCDD/Fs) and NO_x [3–5] in a unique catalytic process (*dDiNOx*), working both as SCR catalyst (Eq. (1)) and oxidizing catalyst (Eq. (2)). This performance makes the catalytic *dDiNOx* process an interesting alternative, to prevent discharge hazardous waste produced by the current containment methods, such as fabric filters, scrubbers and activated carbon beds [6] used currently for PCDD/Fs depuration.

$$4NO + 4NH_3 + O_2 \rightarrow 4N_2 + 6H_2O \quad (1)$$

$$C_{12}H_nCl_8 - nO_2 + (9 + 0.5n)O_2 \rightarrow (n-4)H_2O + 12CO_2 + (8-n)HCl \quad (2)$$

To the best of our knowledge, few studies have reported the combined abatement of NO_x and PCDD/Fs [6–8] by *dDiNOx*. In a previous work [9] we demonstrated the good catalytic performance of VO_x/TiO_2 catalyst in the simultaneous removal of NO and o-dichlorobenzene (o-DCB, a model molecule to simulate PCDD/Fs), although it is rather complex system, since chemical composition of the molecules is completely different and the abatement reactions (Eqs. (1) and (2)) follow different reaction mechanism, not necessarily independent. A tricky balance have to be found, since the high conversion of both pollutants at the same temperature can

* Corresponding author.
E-mail address: asier.aranzabal@ehu.es (A. Aranzabal).

http://dx.doi.org/10.1016/j.apcatb.2016.12.020
0926-3373/

not be reached; the reaction rate of NO reduction is high at low temperature, at which o-DCB oxidation rate is null. However, at higher temperature while o-DCB oxidation sets in, SCR reaction selectivity reduces steadily due to parallel NO and NH_3 oxidation reactions and due to decrement of catalyst acidity. Moreover, the competitive mechanism between NO reduction and o-DCB oxidation reactions for acid and redox sites, leads to reduce the conversion of both pollutants at high temperature (>300 °C) [9,10]. Nonetheless, the NO_2 formed by NO oxidation reaction enhances the o-DCB conversion at low temperature (<300 °C) [9–12]. Then, we concluded that the challenge of *dDiNOx* process is to broaden the operating temperature window, (the temperature range at which the conversion of both pollutants is higher than 60%) both by adjusting operating conditions and by improving catalyst composition.

In a previous work [13] we analyzed metal/zeolites as alternative catalysts since zeolite provides surface acidity and surface area. NO conversion increases notably leading to a broader temperature working window, although o-DCB conversion was substantially lower. In case of VO_x/ZSM5 sample, the bad catalytic performance was due to the formation of big V_2O_5 crystals. The dispersed monomeric [9,14] and polymeric [9,15,16] VO_x species are the most active in o-DCB oxidation and NO reduction, respectively. Many authors agree that interactions between Ti-V promote VO_x spreading, and hence VO_x supported on TiO_2 seems to be the most adequate catalyst among different supports in NO reduction [17,18] and o-DCB oxidation [19] reactions. With the aim of combining the best properties of VO_x/TiO_2 related to dispersed species formation and H-ZSM5 properties associated to acidity and surface area, in this work bifunctional ternary VO_x/TiO_2/ZSM5 catalyst is proposed as alternative to binary VO_x/TiO_2. A systematic investigation varying the TiO_2/ZSM5 ratio will be carried out.

2. Material and methods

2.1. Catalyst preparation

VO_x/TiO_2 (V/Ti) and VO_x/ZSM5 (V/Z) samples were prepared by wet impregnation. The certain amount of precursor (NH_4VO_3) to obtain 3% of vanadium was dissolved in distilled water and complexed with 2 mol of oxalic acid for 1 mol of vanadium. After maintaining the solution slurry at 35 °C and 0.4 kPa under continuous rotation for 3 h, the solvent was evaporated; the resulting samples were dried overnight at 110 °C and then calcined at 500 °C for 3 h (1 °C/min). As a support, commercial TiO_2 anatase calcined at 520 °C for 3 h from Millennium Inorganic Chemicals – Cristal Global (Cristal ACTiVTM G5) was used. The H-ZSM5 support was prepared by calcining the NH_4-ZSM5 zeolite supplied by Zeolyst International (Si/Al molar ratio of 25) in air at 550 °C for 3 h.

$VO_x/XTiO_2$/ZSM5 (V/XTi/Z, being X the TiO_2 mass percent) catalysts were prepared by the wet impregnation method in two steps. Firstly, the desired quantity of Ti(V)butoxy dissolved on *n*-butanol was added to H-ZSM5. After maintaining the solution slurry at 35 °C and 0.4 kPa under continuous rotation for 3 h, the solvent was evaporated. Them, after dried overnight at 110 °C and calcined at 520 °C for 3 h the desired amount of NH_4VO_3 to obtained 3% of V complexed with 2 mol of oxalic acid for 1 mol of V was impregnated. Finally, the samples were dried (110 °C overnight) and calcined at 500 °C for 3 h (1 °C/min). The real metal content of catalysts measured by ICP-AES is summarized in Table 2.

Finally, in order to carry out the catalytic reactions in absence of mass transfer limitations and low pressure drop, the catalysts were pelletized, crushed and sieved to 0.3–0.5 mm. The absence of mass transfer limitation has been checked experimentally elsewhere [13].

2.2. Catalyst characterization

The actual amount of metals (Table 2) in the prepared catalysts were determined by ICP-AES (Horiba Jobin Yvon, Activa) after complete dissolution of the solid samples in 1:3 HNO_3:HCl mixture followed by few drops of HF at 90 °C.

Textural properties were evaluated by means of N_2 adsorption–desorption isotherms, determined at −196 °C in a Micromeritics TRISTAR II 3020 apparatus in case of TiO_2 support and in a Micromeritics ASAP 2010 equipment in case of zeolitic catalysts. The specific surface areas of the prepared samples were determined by the standard BET procedure, using nitrogen adsorption taken in the relative equilibrium pressure interval of 0.03–0.3. In case of zeolitic catalysts the micropores surface area was estimated according to t-plot method using nitrogen adsorption taken in the relative equilibrium pressure interval of 0.012–0.65. Mesopores mean pore size and its distribution were calculated using the BJH method from desorption isotherms. The samples (15–20 mg) were previously degassed under nitrogen flow and under vacuum at 350 °C for 4 h for TiO_2 and zeolite based samples, respectively.

Transmission electron microscopy (TEM) work was done on a Philips SuperTwin CM200 operated at 200 kV and equipped with LaB6 filament and EDAX EDS microanalysis system. The samples for the TEM were prepared by dispersion into ethanol solvent and keeping the suspension in an ultrasonic bath for 5 min, after a drop of suspension was spread onto a TEM copper grid (300 Mesh) covered by a holey carbon film followed by drying under vacuum.

X-ray diffraction (XRD) studies were conducted on a Philips PW 1710 X-ray diffractometer with Cu Kα radiation (λ = 1.5406 Å) and Ni filter. The finely grounded samples were scanned between 10° (2θ) and 70° (2θ) with 0.02°/s sampling interval. Phase identification was conducted by comparison with JCPDS (Joint Committee on Powder Diffraction Standards) database cards.

Catalysts surface acidity was measured by temperature programmed desorption of ammonia (NH_3-TPD) measurements performed on a Micromeritics AutoChem 2910 instrument. Prior to adsorption experiments, the samples (15–20 mg) were pretreated in a quartz U-tube under 5% O_2/He mixture gas flow (50 mL/min) at 500 °C for 45 min, cooled down to 100 °C and treated with helium (50 mL/min) for 60 min. The adsorption step was performed by admitting small pulses of ammonia in helium (10% NH_3/He) at 100 °C up to saturation. Subsequently, the samples were exposed to a flow of helium (50 mL/min) for 2 h at 100 °C in order to remove reversibly and physically bound ammonia from the surface. Finally, TPD was started using helium as carrier gas (50 mL/min) from 100 to 550 °C at a heating rate of 10 °C/min, while the ammonia desorption was continuously monitored with a TCD detector. The amount of ammonia desorbed was determined by time integrated NH_3-TPD curves as a measure of the acid site concentration.

Redox behavior was examined by temperature programmed reduction using H_2 (H_2-TPR). The experiments were conducted on a Micromeritics AutoChem 2920 instrument. Firstly, all the samples (15–20 mg) were pre-treated under 50 mL/min of 5% O_2/He mixture at 500 °C for 45 min and then cooled down to room temperature and flushed with helium for 60 min. Then samples were heated from room temperature to 1000 °C at a rate of 10 °C/min under a 50 mL/min of 5% H_2/Ar mixture gas flow. The water produced by reduction was trapped in a cold trap, and the consumption of H_2 was continuously monitored with a TCD detector. The total amount of H_2 consumption was calculated from time integrated H_2-TPR curves.

The Raman spectroscopy was performed in an Olympus DX40 Raman spectroscope. The 633 nm laser was used and for each spectrum, 10 s were employed and 30 scans were accumulated in the spectral window from 140 to 1200 cm^{-1}. The analyses

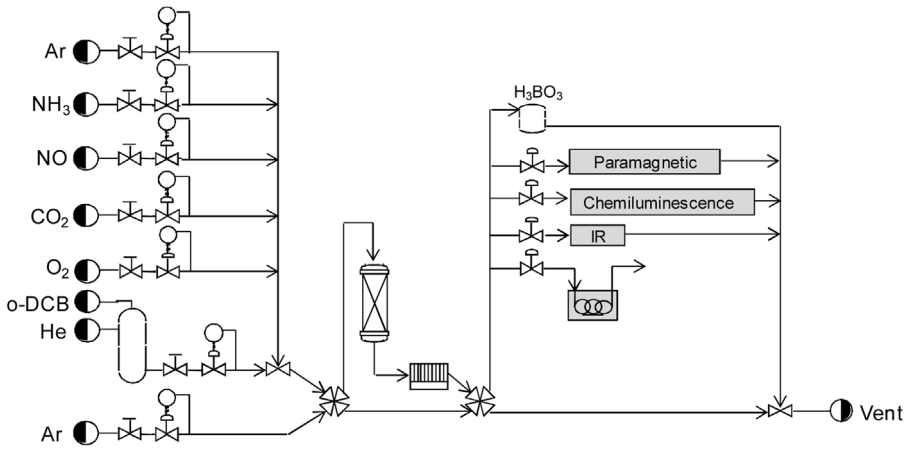

Fig. 1. Experimental set-up.

were performed at 400 °C on fluidization reactor on sieved from (0.05–0.2 nm) and under 20 mL/min air flow after kept samples dehydrating for 3 h.

2.3. Experimental reaction set-up and catalytic tests

The experimental reaction set-up is shown in Fig. 1. The gas mixture was fixed in order to simulate as best as possible the MWI real feed. Due to the difficulty of handling such toxic PCDD/Fs, researchers usually work with less toxic model molecules and with a chemical structure similar to that of PCDD/Fs such a o-dichlorobenzene (o-DCB) [19,20]. Thus, the catalytic reactor feed consisted of O_2 (10%), CO_2 (10%), NO (300 ppm), NH_3 (300 ppm), o-DCB (100 ppm) and balanced Ar. The gas flows were regulated by gas mass flow controllers (Bronkhorst® High-Tech F-201CV) whereas o-DCB liquid stream was dosed by a Bronkhorst® High-Tech μ-Flow L01-AAA-99-0-20S mass flow controller. The complete evaporation of the liquid stream and homogenous blend with the gas stream was performed in a controlled-evaporator-mixer (Bronkhorst® High-Tech W-102A-111-K). In order to avoid gas adsorption and condensation in the pipes, these were heated with electrical resistances. The resulting gaseous stream went through the fixed catalytic bed inside a U-shaped tubular quartz reactor (13.6 mm), which was heated into a convective-flow oven. Before catalytic measurement, the fixed bed was dried at 200 °C during 2 h in pure argon flow (2 L_N/min). Catalytic tests were performed as light-off curve 1.5 atm pressure by feeding constant total flow of 2 L_N/min and increasing temperature from 100 to 500 °C with a constant heating rate of 1.5 °C/min. The catalytic bed consisted of 1.5 g of particulate catalysts (0.3–0.5 mm) mixed with inert quartz (0.5–0.8 mm) in order to fill a bed volume of 3 mL, resulting in a GHSV value of 40 000 h^{-1}.

An on-line gas chromatograph (Agilent Technologies 7890A) equipped with a HP-VOC capillary column and a mass selective detector 5975C was used to quantify o-DCB concentration in the reactor inlet and outlet streams and also to detect possible reaction hydrocarbon sub-products. Furthermore, NO was continuously measured using chemiluminescence analyzer. CO_2, CO and N_2O were analyzed with infrared, whereas O_2 with paramagnetic detector, all of them integrated in NGA 200 Rosemount Analytical analyzers. During the reaction it was difficult to follow NH_3 due to its reaction with HCl (product of o-DCB oxidation) and the subsequent NH_4Cl formation. For this, NH_3 was only measured before reaction to verify its concentration by titration. The feed, without CO_2, was passed through a solution of boric acid (0.005 M) for some time and then, the amount of ammonia which reacted with boric acid was determined by measuring the amount of hydrochloric acid solution (0.1 N) required to bring the pH to its initial value. Phenol Red, with a pH range of 6.6 (yellow)–8.0 (red), was used as an indicator.

Catalytic test reproducibility was performed by repeating the same light-off test (control test) regularly as shown elsewhere [9]. NO conversion exhibits a constant standard deviation around 1.5% in the whole range of temperature. However, standard deviation of o-DCB conversion increases up to 5% as the slope of the light-off curve increases, due to the high sensitivity of o-DCB oxidation to the temperature.

3. Results and discussion

Fig. 2 shows the conversion of o-DCB and NO as a function of the reaction temperature over the reference V/Ti and zeolite based catalysts. Conversion of o-DCB shows the typical S-shape. V/Ti is the most active catalyst for o-DCB oxidation in the whole range of temperature, closely followed by V/46Ti/Z and V/28Ti/Z, respectively. The temperatures required for the same o-DCB conversion (T_{50}) over V/46Ti/Z and V/28Ti/Z catalysts are respectively 20–25 °C and 50–60 °C higher than the reference V/Ti catalyst. The activity of V/13Ti/Z and V/Z is far lower than V/Ti as to consider an alternative. Even so, V/46Ti/Z and V/28Ti/Z are more active than Cu/Z (35–40 °C) and Mn/Z (85–90 °C) tested elsewhere [13], which suggests that Ti-V interactions might be the key factor for the o-DCB oxidation, while the contribution of zeolites higher acidity is considerably lower.

The conversion of NO shows a particular shape that can be divided in three zones (zone I, II and III). The low temperature range (zone I) is described exclusively by standard SCR reaction (Eq. (1)), since the typical SCR conditions, such as NO/NH_3 ratio of 1 and excess of O_2 exist [2,18]. In this range V/Ti catalyst is still the most active catalyst (T_{50} = 150 °C), closely followed by V/46Ti/Z (T_{50} = 165 °C) and V/28Ti/Z (T_{50} = 180 °C). V/Z (T_{50} = 205 °C) and V/13Ti/Z (T_{50} = 240 °C) are respectively much less active.

In the light-off region, both for o-DCB oxidation and for NO reduction, the activity of the ternary $VO_x/TiO_2/ZSM5$ catalysts increases notably by increasing the amount of TiO_2. The high activity of V/46Ti/Z sample could be due to the good VO_x dispersion in the proximities of TiO_2, since many authors agree that TiO_2 is the most adequate support for NO reduction [17,18] and o-DCB oxidation [19] because interactions between Ti-V promote the spreading of VO_x.

The outstanding feature of zeolite based catalysts is the peak conversion of NO at the end of the light-off (zone II), which is significantly higher over all the zeolites than over the reference V/Ti catalyst. At most, 68% of NO conversion is obtained at 180 °C with commercial type V/Ti catalyst, whereas almost 100% is obtained

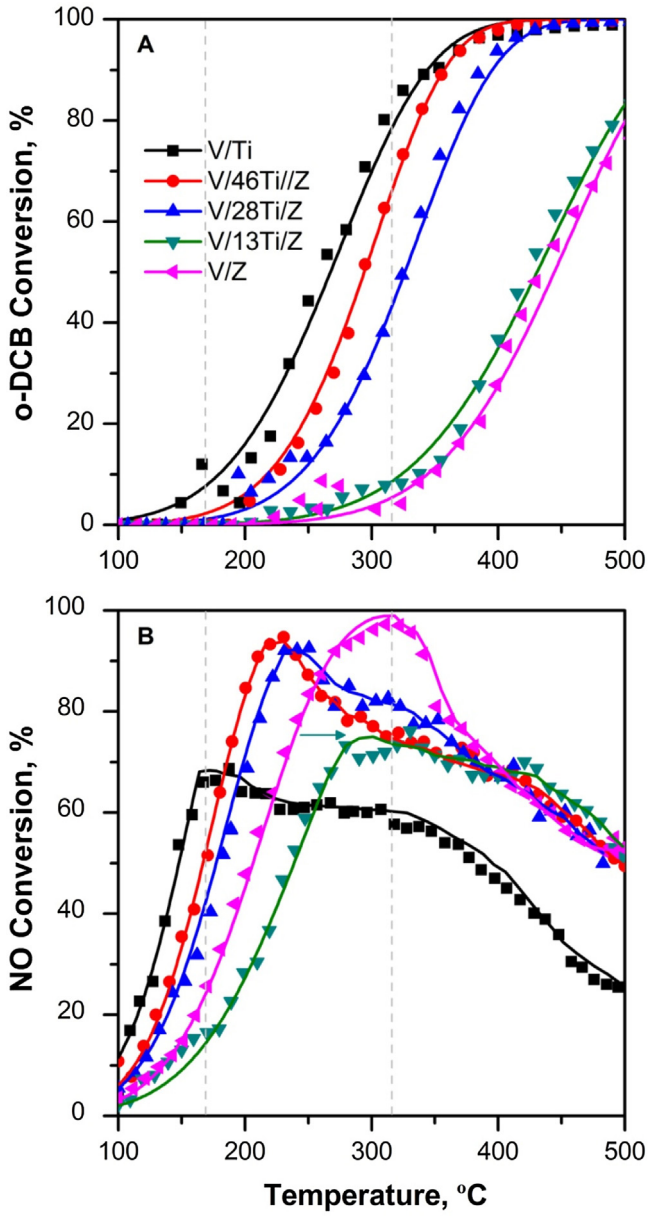

Fig. 2. Conversion of A) o-DCB and B) NO (100 ppm o-DCB, 300 ppm NO, 300 ppm NH_3, 10% O_2, 10% CO_2, 2 L_N min^{-1}, 1.5 atm and 80 $L_N \cdot (h\,g)^{-1}$).

with V/Z at 300 °C, followed by V/46Ti/Z (95%, 220 °C) and V/28Ti/Z (91%, 235 °C). The peak conversion of V/13Ti/Z is slightly higher than the reference V/Ti but at much higher temperature (70%, 280 °C).

The higher NO conversion of V/46Ti/Z and V/28Ti/Z, and the moderate conversion of o-DCB at middle-high temperature (zone II) leads to broaden notably the temperature working window, which is define as the temperature range where the conversion of both pollutants is higher than 60%. As summarized in Table 1, the temperature working window of V/Ti is only 45 °C, while it is increased up to 145 °C in case of V/46Ti/Z sample and 110 °C in the case of V/28Ti/Z. However V/Z sample is not a suitable catalysts for *dDiNOx* since it is not possible to convert both pollutants simultaneously (working window 0 °C). V/13Ti/Z is also excluded as an alternative due to the high temperature of NO peak conversion and low conversion of o-DCB, resulting in a narrow working window (20 °C) at high temperature (450–470 °C).

At higher temperature (zone III), the acidity of the catalyst decreases and NH_3 tends to oxidize (Eq. (3)) rather than to adsorb on Brøsnted acid sites. Consequently, over NO peak conversion temperature, NO conversion drops moderately or drastically, depending on the relative competitive reaction rates over each particular sample.

$$4NH_3 + 5O_2 \rightarrow 4NO + 6H_2O \quad (3)$$

Although the general effects are well described in the literature, the shape of the NO_x conversion over V/Ti is rather different to the literature, which usually a steady increase is seen up to around 375 °C followed by a almost symmetrical decrease at higher temperatures [2,18,21,22]. In order to explain this difference we analyzed three possible hypotheses. The first hypothesis was an experimental failure, which was discarded due high reproducibility of the light-off curve [9]: NO conversion exhibits a constant standard deviation around 1.5% in the whole range of temperature. However, standard deviation of o-DCB conversion increases up to 5% as the slope of the light-off curve increases, due to the high sensitivity of o-DCB oxidation to the temperature.

The second hypothesis was the effect of o-DCB oxidation, which was taking place simultaneously in the reactor, unlike the other works in the literature. Then, we performed experiments with and without simultaneous oxidation of o-DCB (Fig. 3A). We found some competition when both reactions occurred simultaneously, leading to lower NO conversion, compared to independent NO reduction. However the shape of NO conversion was rather similar.

The third hypothesis was based on in the way of reactor heating to obtain the light-off curve. We found that in most of the works [2,18,21,22] the temperature was increased by steps and the conversion was measured once the reactor's temperature was stabilized. However, in this work the temperature was raised steadily by a rate of 1.5 °C/min. Then we repeated the simultaneous NO reduction and o-DCB oxidation by rising the temperature by steps of 20 °C, and measuring conversions once the reactor's temperature was stabilized. The Fig. 3B compares the NO conversion curves obtained by different ways of rising reaction temperature. In both cases the NO conversion at low temperature (100–150 °C) is the same. In this range the NO conversion is low and only SCR reaction (Eq. (1)) is taking place. On the contrary, at middle temperature range (150–350 °C) the conversion curves are different. The curve obtained by heating in stages increases steadily up to rounded maximum and above such temperature decreases steadily, resulting in symmetrical shaped conversion curve as shown by cited works [2,18,21,22]. However, when reactor is heated steadily, the NO conversion goes on increasing with the temperature at the same rate as in the lower temperature range, up to a sharp peak (150–185 °C), above which, peak temperature conversion decreases notably. There could be two reasons for this: either because there is heating inertia and/or SCR is an exothermic reaction leading to hot pots in the catalyst sites. On the contrary, when the reaction temperature is controlled and stabilized by stages, the inertia and the effect of hot pots are minimized.

The higher NO peak conversion over zeolite based samples is most likely due to the acid sites provided by the zeolite [13,23]. The higher acidity of zeolites is confirmed by NH_3-TPD measurements (Table 2). Zeolite based samples are between 2 and 3 times more acid than V/T catalyst (0.23 mmol NH_3/g). We found an asymptotic increase of NO conversion with respect to the amount of acid sites, up to a maximum of 0.79 mmol NH_3/g for metal/zeolites (V > Mn > Cu > Fe) elsewhere [13]. Although the binary V/Z sample (0.79 mmol NH_3/g) is the most acid sample (and highest NO peak conversion), the correlation between acidity level and NO peak conversion among VO_x/TiO_2/ZSM5 samples is not direct, which suggest there are additional properties contributing to the NO peak

Table 1
Activity measurements results.

	Working window, °C	Ea, KJ/mol		Maximum Concentration, ppm		
		NO	o-DCB	CO	TCB[a]	N_2O
V/Ti	285–330 (45)	47.2 ± 0.70	43.4 ± 2.30	320	0	120
V/46Ti/Z	305–450 (145)	49.0 ± 0.50	56.7 ± 1.44	215	0	80
V/28Ti/Z	340–450 (110)	45.4 ± 0.34	57.9 ± 2.55	200	0	75
V/13Ti/Z	450–470 (20)	40.3 ± 0.34	61.4 ± 2.94	150	0	35
V/Z	–	43.2 ± 0.24	69.1 ± 2.21	100	0.5	20

[a] An arbitrary value based on standards liquids patrons in GC–MS.

Table 2
Characterization results.

	Chemical composition		Textural properties				Acid property	
	V, wt.%	TiO_2,wt.%	S_{BET},$m^2\ g^{-1}$	S_{micro}, $m^2\ g^{-1}$	V_p, $cm^3\ g^{-1}$	D_p, Å	NH_3 mmol g^{-1}	B/L
V/Ti	2.94	94.7	58.9	–	0.24	128	0.23	0.55
V/46Ti/Z	3.06	46.4	205	104	0.19	81.5	0.46	0.38
V/28Ti/Z	3.02	28.3	281	115	0.21	57.7	0.55	0.93
V/13Ti/Z	2.64	13.1	358	160	0.21	55.0	0.63	1.11
V/Z	3.42	–	361	193	0.19	56.6	0.79	1.32
TiO_2	–	100	70	–	0.22	122	0.17	0.02
H-ZSM5	–	–	390	200	0.19	53.3	0.60	3.39

conversion, very likely associated to the dispersion of both TiO_2 and VO_x.

The contribution of zeolites' external surface area (200–400 m^2/g) to the catalytic activity with respect to the reference V/Ti (60 m^2/g) does not seem to be a key factor to explain the higher NO peak conversion and the wider operating temperature window. The N_2 isotherms of bare supports (TiO_2 and H-ZSM5) and prepared catalysts are compared in Fig. 4. The TiO_2 and accordingly the reference V/Ti are mesoporous materials while zeolite based catalysts are microporous. The increase of TiO_2 loading leads to reduce the BET area and especially microporous surface area [24] (Table 2). The BET area decreases from 360 (V/Z) to 205 m^2/g (V/46Ti/Z). Nonetheless, TiO_2 addition shows low impact in the catalysts textural properties. The N_2 isotherms of VO_x/TiO_2/ZSM5 samples fit properly to type I according to IUPAC characteristic of microporous materials, even when 46 wt.% of TiO_2 is added.

Contrarily, XRD patters of the samples shown in Fig. 5 show that the intensity of the diffraction peaks associated to H-ZSM5 crystalline structure decreases drastically as TiO_2 content increases. Accordingly, the intensity of anatase most intense diffraction peaks increases. The impregnation of TiO_2 as anatase crystalline is also characterized by intense Raman bands at 630 cm^{-1} as well as 395 and 510 cm^{-1} (not shown) [16,25,26] (Fig. 7). The fact that crystalline structure is mostly defined by anatase while textural properties are mostly defined by H-ZSM5, suggest that TiO_2 is mainly deposited on the zeolite external surface area.

The low impact of TiO_2 on zeolites' textural properties, even with 46 wt.% of TiO_2, is clearly visible in the TEM images (Fig. 6), where the zeolite raw structure is largely intact. This fact suggests that TiO_2 is heterogeneously dispersed over H-ZSM5, from well-defined small particles, as in V/13Ti/Z with a size ca. 7 nm, to big clusters, predominant in V/28Ti/Z and V/46Ti/Z samples. The resulting TiO_2 dispersion is lower than the expected [27], considering of high surface area of H-ZSM5. This fact could explain the

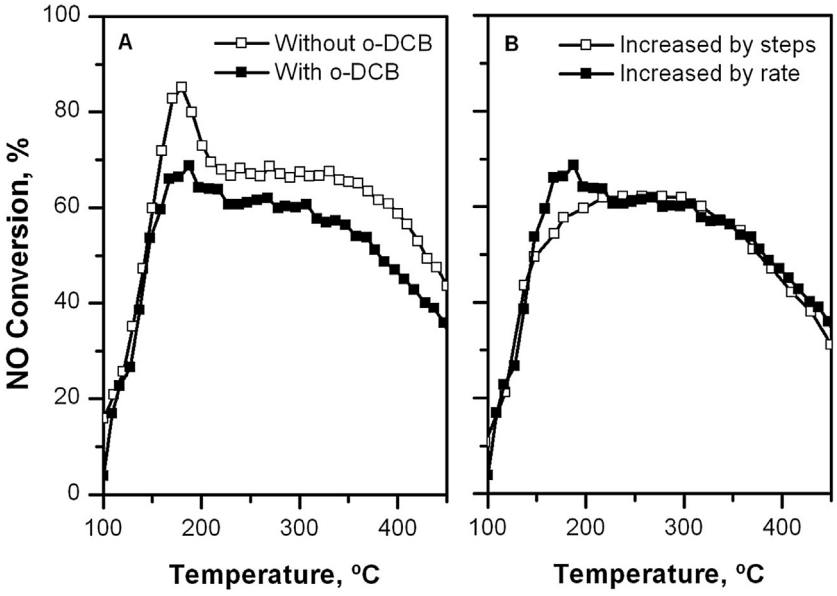

Fig. 3. NO conversion B) with and without o-DCB in gas feeding B) rising the temperature by constant rate and by steps.

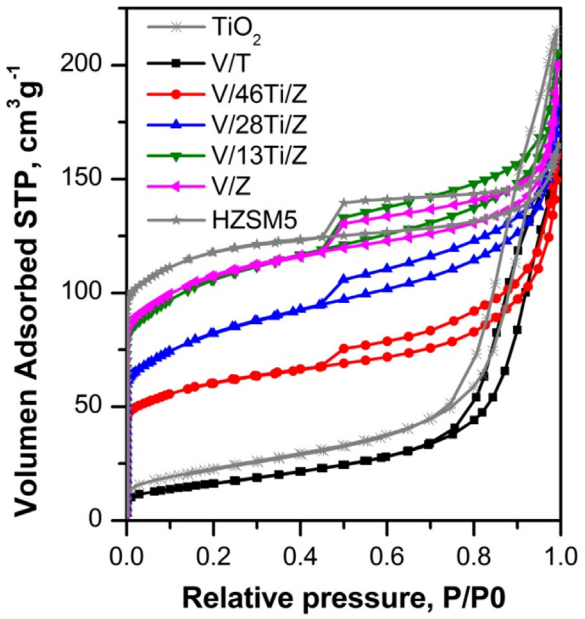

Fig. 4. Isotherms of VO_x/TiO_x/ZSM5 catalysts.

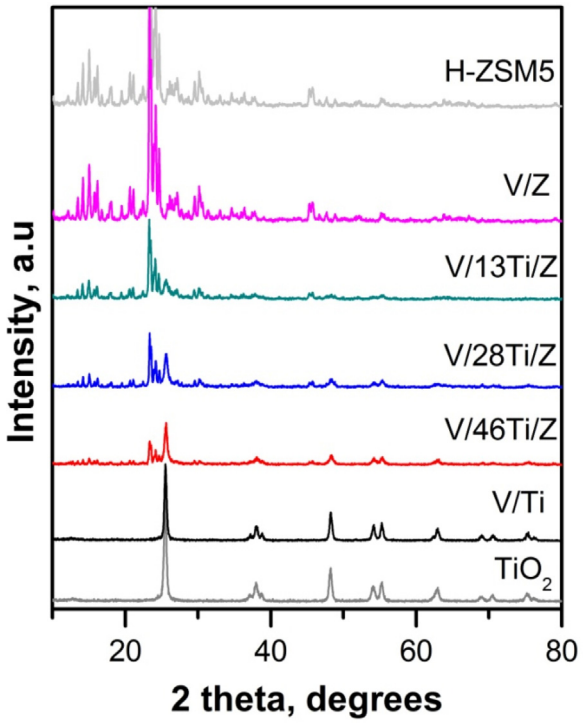

Fig. 5. XRD of VO_x/TiO_x/ZSM5 catalysts.

low impact of the high surface area in the activity of the ternary samples, as compared with V/Ti sample. Nevertheless, the addition of high amount of titanium on VO_x/TiO_2/ZSM5 samples, might allow improving VO_x dispersion, through Ti-V interaction [17–19], which is a key factor in the conversion of both o-DCB and NO, as we reported elsewhere [9]: the polymeric VO_x species are the most active species for NO reduction, while isolated monomerics for o-DCB oxidation; crystalline species are much less active.

TEM images show big V_2O_5 crystalline species characterized by sharp edges due to their octahedral or pyramidal coordination [28], in V/Z and V/13Ti/Z samples, while EDX spectra show high dispersion of VO_x over high TiO_2 samples (V/28Ti/Z, V/46Ti/V and V/Ti). In this analysis the Ti K_β and V K_α emission lines overlap in EDX spectrum, so to determine the presence of vanadium the relative X-ray intensities of Ti K-shell were taken into account, where IKα/IKβ is 0.1 [29]. An important deviation of this value indicates that vanadium is present in the analyzed area.

Raman spectra also show clear evidences of improved V_2O_5 dispersion, characterized by the intensity reduction of the band at 995 cm^{-1} [16,25,26], as the TiO_2 content is increased. This band is indicative of the presence of crystalline V_2O_5 [16,25,26]. In agreement with TEM images, its intensity is very high in V/Z sample and clearly decreases by the TiO_2 loading.

In spite of the overlapping of the Raman band at 1025–1030 cm^{-1} characteristic of V=O stretching [16,25,26] in isolated species (either monomeric or polymeric) and the H-ZSM5 broad band, the tightening of the band with the TiO_2 loading (Fig. 7B) suggests the increase of disperse VO_x species. The broad band near 940 cm^{-1} associate to V-O-V by the classical assignment [16,25,30] also overlaps with H-ZSM5 Raman band, but the comparison of these bands between high TiO_2 content catalysts, which zeolite contribution is nil or very low in the spectra (V/Ti, V/46Ti/Z and V/28Ti/Z), suggests that the intensity and accordingly the contribution of polymeric species also increases with TiO_2 content.

H_2-TPR measurements were performed to quantify the distribution of different VO_x species. The reduction peak of VO_x/TiO_2/ZSM5 samples (Fig. 8) can be deconvoluted into three symmetric Gaussian peaks [9,25]. The lower temperature reduction peak could be related to monomeric VO_4 species reduction, the middle reduction peak can be associated to two dimensional polymeric species reduction and the higher reduction step is due to crystalline V_2O_5 species reduction [28,31,32]. Fig. 9 shows the relative amount of each species as a function of Ti/V ratio, assuming that VO_x dispersion could directly relate to Ti-V interactions or bonds [28,33].

The contribution of crystalline V_2O_5 decreases linearly as Ti/V ratio increases. Accordingly, the proportion of isolated monomeric and polymeric species increases. Isolated monomerics are preferably formed with low TiO_2 loads (13%, Ti/V=5) while polymeric species contribution increases significantly with high TiO_2 loads (46%, Ti/V=15). This fact suggests that VO_x is spreading in the proximities of TiO_2; few Ti-V interactions (low Ti) promotes isolated species formation while many interactions (high Ti) leads to agglomerates development. We reported similar effect over V/T samples with respect to the vanadium loading [9,25].

Fig. 10 confirms Ti-V interaction in the ternary VO_x/TiO_2/ZSM5 is the key factor in their specific activity. The TOF was estimated by assuming the first order reaction rate as in Eq. (4):

$$TOF = F_0 \cdot \ln(1-X_A)/(W \cdot X_V/MW_V \cdot P') \quad (4)$$

where F_0 is the reactive initial molar flow, X_A is the reactive conversion, W is the weight of catalyst, X_v is the catalyst vanadium mass fraction, MW_v is vanadium molecular weight and P' is the relative pressure.

The first order reactions are assumed in the literature for NO reduction [34,35] and o-DCB oxidation [36,37] and Fig. 2 shows that both reactions are acceptably described by the first order kinetic also in *dDiNOx* process, noted by the low deviation of the experimental data (symbols) from the first order kinetic equation (solid line).

As expected, the catalytic activity of both reactions increases with TiO_2 addition and a linear relationship exists between the TOF and the theoretical number of Ti-V interactions (Ti/V ratio). The TOF of V/13Ti/Z (Ti/V=5) is data point with highest deviation from the straight line, especially in case of SCR reaction. By H_2-TPR profiles deconvolution (Figs. 8 and 9) it has been suggested that the contribution of polymeric $(VO)_n$ species is the lowest in V/13Ti/Z

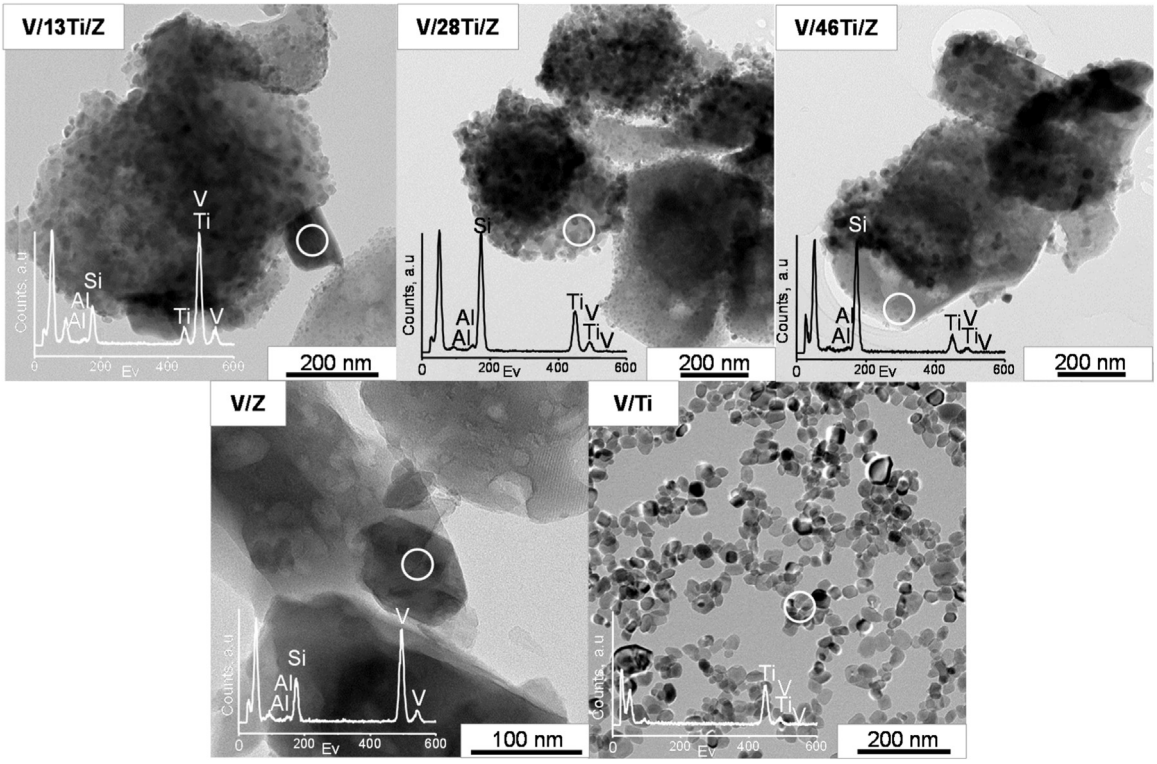

Fig. 6. TEM-EDX micrographs for VO_x/TiO_x/ZSM5 catalysts.

sample, since anatase particles act as a single support, forming firstly monomeric VO_x species and then polymerics on its proximities. Then, the lowest activity of V/13Ti/Z in NO reduction reaction is explained by the lowest contribution of polymeric species. This fact confirms the highest activity of these species in SCR reaction concluded in a previous work [9].

Another advantage of ternary VO_x/TiO_2/ZSM5 alternative catalysts is the lower selectivity to undesired byproducts, such as CO and N_2O. Table 1 summarized the maximum concentration recorded over all the catalysts. The formation profile of CO over VO_x/TiO_2/ZSM5 catalysts, shows almost identical shape as the reference VO_x/TiO_2 [9]; its formation occurs in the temperature range that o-DCB is being oxidized with a selectivity ca. 40%. On the contrary, N_2O formation profile is shifted to lower temperature as the TiO_2 loading decreases. N_2O formation at low temperature occurs via NH_4NO_3 intermediate decomposition and the lower formation

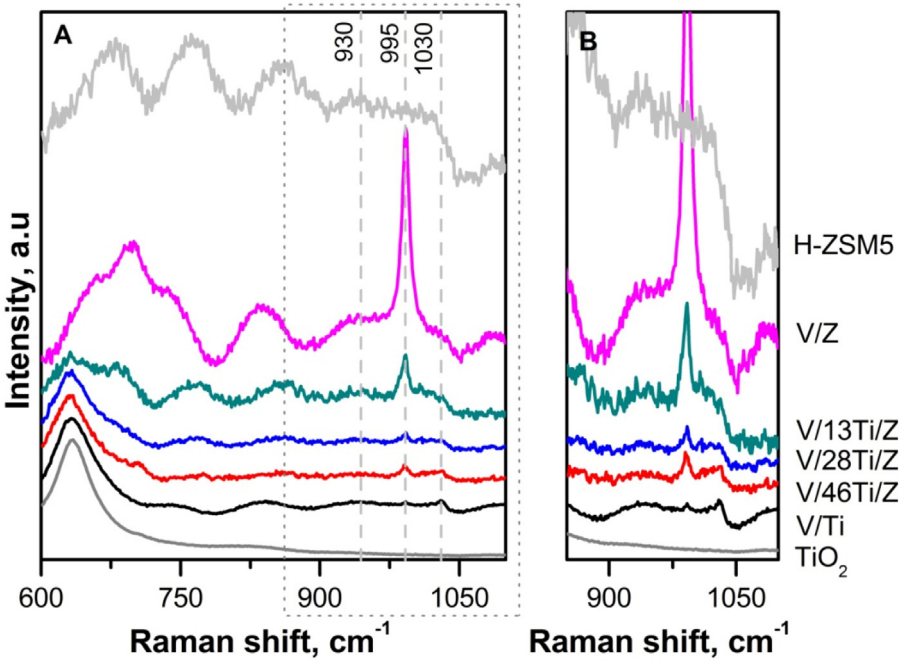

Fig. 7. Raman spectra of VO_x/TiO_x/ZSM5 catalysts.

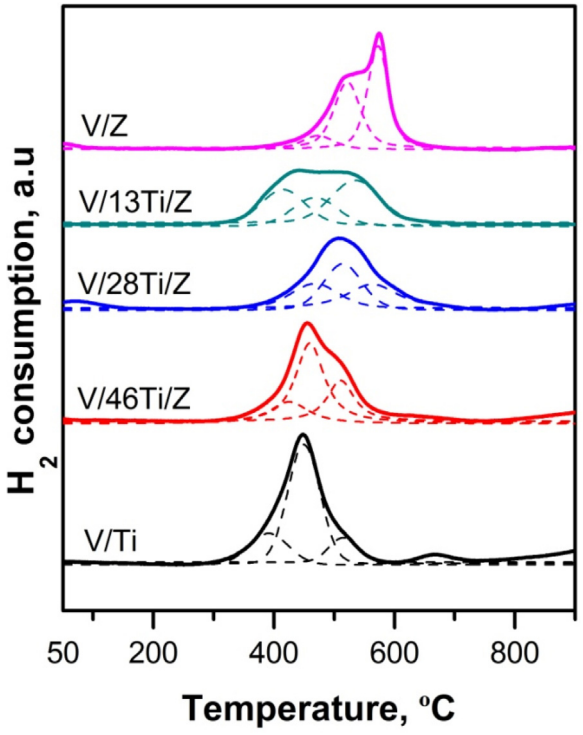

Fig. 8. H_2-TPR profiles of VO_x/TiO_x/ZSM5 catalysts.

of it over zeolites could be due to higher stability of NH_4NO_3 within the smaller pores [38]. The zeolite narrow pore size also makes difficult the diffusion of big molecules such as o-DCB inside the pores, and hence chlorination reactions occur [39,40], detecting traces of 1,3,5-triclorobencene (TCB) over V/Z catalyst. We also found high amount of TCB over Cu/zeolite and Mn/zeolite [13], so it can be concluded that the Ti-V interaction also avoids its formation.

This work was performed under dry inlet conditions, though waste incineration typically leads to 10–20% H_2O in the gas. Although, the influence of water addition to the feed stream is beyond the scope of this study, future work should be devoted to analyze the effect of water on the conversion and selectivity of

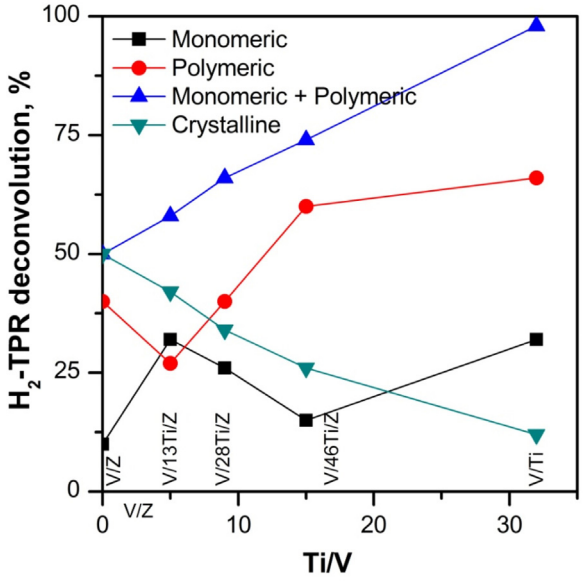

Fig. 9. Deconvolution of H_2-TPR profiles as a function of Ti/V ratio.

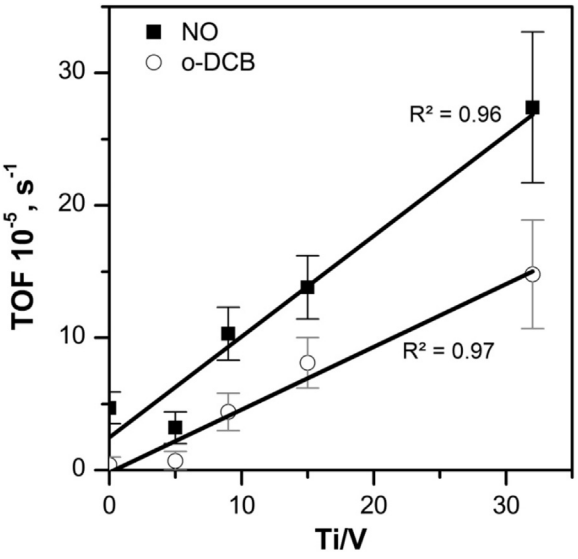

Fig. 10. The TOF of NO reduction (150 °C) and o-DCB oxidation (300 °C) as a function of Ti/V over VO_x/TiO_2/ZSM5 catalysts.

NO_x reduction and o-DCB oxidation. Due to the affinity of water molecules to acid sites, a general decrease of NO conversion is expected [22,41], but at low temperature an increase of o-DCB conversion is also expected [42,43]. The effect of SO_2 on catalyst stability and durability should be also analyzed.

4. Conclusions

A series of VO_x/TiO_2/ZSM5 were prepared in order to enhance to redox and acid functionalities of commercially used VO_x/TiO_2 for the combined abatement of NO and o-DCB from the off-gases of a MSW incinerator plant. The catalysts have been prepared by wet impregnation in two steps with a constant concentration 3% of V and varying the TiO_2 content from 0 to 46%. VO_x/TiO_2 was also prepared as a reference sample. The ternary VO_x/TiO_2/ZSM5 samples (V/46Ti/Z and V/28Ti/Z) provides superior NO conversion, which allows wider operating temperature working window, at which more than 60% conversion both for o-DCB and NO is achieved; although conversion of o-DCB is slightly lower than the reference VO_x/TiO_2. The sample with low TiO_2 loading (V/13Ti/Z) also provides superior NO conversion than the reference VO_x/TiO_2, but at temperatures considerably higher. Conversely, conversion of o-DCB is significantly lower, so the temperature working window is even narrower than the reference VO_x/TiO_2 sample.

A deep catalysts characterization (N_2 adsorption-desorption isotherms, XRD, TEM, NH_3-TPD, H_2-TPR and Raman) allows us to conclude that the higher NO peak conversion over zeolite based samples is partly due to higher amount of acid sites provided by the zeolite and partly due to Ti-V interaction, which is a key factor in the conversion of both o-DCB and NO. We found that TiO_2 is heterogeneously dispersed over zeolilte, but VO_x dispersion is enhanced as the TiO_2 content is increased, leading to a higher active polymeric species contribution, as in the sample V/46Ti/Z (confirmed by correlation between TOF and Ti-V interaction). Additional evidence of this fact, is the lower activity of other metal/zeolites (Cu, Mn, V, Fe) [13], although they share the characteristic of higher NO peak conversion than the reference VO_x/TiO_2, due to the enhanced acidity of the zeolite. We also found that the V-Ti interaction also avoids the formation of highly chlorinated subproducts, such us, trichlorobencene, as we found in samples like Cu/Z, Mn/Z, etc. [13].

Finally, it is remarkable that the TiO_2 dispersion is lower than the expected, considering the high surface area of H-ZSM5, which

gives rise to opportunities to research on this topic so as to enhance the dispersion of highly active Ti-V interactions over zeolite surface, and hence highly increase conversion of both o-DCB and NO.

Acknoledgments

This research was funded by Basque Government though the Grant to Consolidated Research Groups (GIC-07/67-JT-450-07) and the SAIOTEK program (S-PE11UN074), by University of the Basque Country UPV/EHU through the UFI (UFI 11/39) and the Grant for the acquisition and renovation of scientific infrastructure (INF12/37) and by the Spanish Ministry of Economy and Competitiveness (CTM2012-31576). One of the authors (M. Gallastegi-Villa) acknowledges also the Basque Government for the PhD Research Grant (BFI-2011-238). The authors would also like to thank the technical and human support from UPV/EHU Advanced Research Facilities (SGIker) in XRD (A. Larrañaga) and Haldor Topsøe A/S (S.B. Rasmussen) in Raman. Millennium Inorganic Chemicals – Cristal Global is also acknowledged for kindly supplying TiO_2 (CristalACTiV^{TM} G5).

References

[1] A. Bosmans, I. Vanderreydt, D. Geysen, L. Helsen, J. Clean. Prod. 55 (2013) 10–23.
[2] R.M. Heck, Catalytic abatement of nitrogen oxides–stationary applications, Catal. Today 53 (1999) 519–523.
[3] K. Sam-Cwan, J.S. Hwan, J. Il-Rok, K. Ki-Hun, K. Myung-Hee, K. Jae-Hyung, Y. Jun-Heung, K. Seung-Jin, Y. Jae-Cheon, J. Dong-Hee, Chemosphere 43 (2001) 773–776.
[4] H.C. Wang, J.F. Hwang, K.H. Chi, M.B. Chang, Chemosphere 67 (2007) S177–S184.
[5] Directive 2000/76/EC of the European Parliament and of the Council of 4 December 2000 on the incineration of waste.
[6] E. Finocchio, G. Busca, M. Notaro, Appl. Catal. B 62 (2006) 12–20.
[7] J. Jones, J.R.H. Ross, Catal. Today 35 (1997) 97–105.
[8] M. Goemans, P. Clarysse, J. Joannès, P. De Clercq, S. Lenaerts, K. Matthys, K. Boels, Chemosphere 50 (2003) 489–497.
[9] M. Gallastegi-Villa, A. Aranzabal, Z. Boukha, J.A. González-Marcos, J.R. González-Velasco, M.V. Martínez-Huerta, M.A. Bañares, Catal. Today 254 (2015) 2–11.
[10] G. Su, Catal. Sci. Technol. 5 (2015) 1041–1051.
[11] Z. Xu, S. Deng, Y. Yang, T. Zhang, Q. Cao, J. Huang, G. Yu, Chemosphere 87 (2012) 1032–1038.
[12] F. Bertinchamps, M. Treinen, N. Blangenois, E. Mariage, E.M. Gaigneaux, J. Catal. 230 (2005) 493–498.
[13] M. Gallastegi-Villa, A. Aranzabal, J.A. González-Marcos, J.R. González-Velasco, Appl. Catal. B 184 (2016) 238–245.
[14] C. Gannoun, R. Delaigle, P. Eloy, D.P. Debecker, A. Ghorbel, E.M. Gaigneaux, Catal. Commun. 15 (2011) 1–5.
[15] I.E. Wachs, G. Deo, B.M. Weckhuysen, A. Andreini, M.A. Vuurman, M.d. Boer, M.D. Amiridis, J. Catal. 161 (1996) 211–221.
[16] I. Giakoumelou, C. Fountzoula, C. Kordulis, S. Boghosian, J. Catal. 239 (2006) 1–12.
[17] M.A. Reiche, E. Ortelli, A. Baiker, Appl. Catal. B. 23 (1999) 187–203.
[18] G. Busca, L. Lietti, G. Ramis, F. Berti, Appl. Catal. B. 18 (1998) 1–36.
[19] F. Bertinchamps, C. Grégoire, E.M. Gaigneaux, Appl. Catal. B. 66 (2006) 1–9.
[20] M.A. Larrubia, G. Busca, Appl. Catal. B. 39 (2002) 343–352.
[21] J. Wang, Z. Yan, L. Liu, Y. Chen, Z. Zhang, X. Wang, Appl. Surf. Sci. 313 (2014) 660–669.
[22] M.D. Amiridis, I.E. Wachs, G. Deo, J.M. Jehng, D.S. Kim, J. Catal. 161 (1996) 247–253.
[23] S.S.R. Putluru, A. Riisager, R. Fehrmann, Appl. Catal. B 97 (2010) 333–339.
[24] S. Cimino, L. Lisi, M. Tortorelli, Chem. Eng. J. 283 (2016) 223–230.
[25] D.A. Bulushev, L. Kiwi-Minsker, F. Rainone, A. Renken, J. Catal. 205 (2002) 115–122.
[26] M.V. Martínez-Huerta, J.L.G. Fierro, M.A. Bañares, Catal. Commun. 11 (2009) 15–19.
[27] I. Jansson, S. Suárez, F.J. Garcia-Garcia, B. Sánchez, Appl. Catal. B 178 (2015) 100–107.
[28] I.E. Wachs, B.M. Weckhuysen, Appl. Catal. A 157 (1997) 67–90.
[29] J. Goldstein, D.E. Newbury, D.C. Joy, C.E. Lyman, P. Echlin, E. Lifshin, L. Sawyer, J.R. Michael (Eds.), Scanning Electron Microscopy and X-ray Microanalysis, third ed., Springer, New York, 2003.
[30] C. Freitag, S. Besselmann, E. Löffler, W. Grünert, F. Rosowski, M. Muhler, Catal. Today 91–92 (2004) 143–147.
[31] G.C. Bond, Appl. Catal. A 157 (1997) 91–103.
[32] S. Besselmann, C. Freitag, O. Hinrichsen, M. Muhler, Phys. Chem. Chem. Phys. 3 (2001) 4633–4638.
[33] G.C. Bond, S.F. Tahir, Appl. Catal. 71 (1991) 1–31.
[34] B.K. Yun, M.Y. Kim, Appl. Therm. Eng. 50 (2013) 152–158.
[35] L. Lietti, I. Nova, E. Tronconi, P. Forzatti, Catal. Today 45 (1998) 85–92.
[36] S. Krishnamoorthy, J.A. Rivas, M.D. Amiridis, J. Catal. 193 (2000) 264–272.
[37] G. Wielgosiński, A. Grochowalski, T. Machej, T. Pająk, W. Ćwiąkalski, Chemosphere 67 (2007) S150–S154.
[38] Z. Chen, M. Wei, F. Kollar, Y. Wang, J. Szanyi, C.H.F. Peden, J. Catal. 329 (2015) 490–498.
[39] S. Sharma, S.G. Hegde, A.P. Singh, Appl. Catal. A 162 (1997) 201–211.
[40] S. Scirè, S. Minicò, C. Crisafulli, G. Burgio, V. Giuffrida, Stud. Surf. Sci. Catal. 142 (2002) 1023–1030.
[41] I. Nova, L. Lietti, E. Tronconi, P. Forzatti, Catal. Today 60 (2000) 73–82.
[42] C.E. Hetrick, F. Patcas, M.D. Amiridis, Appl. Catal. A 101 (2011) 622–628.
[43] F. Bertinchamps, A. Attianese, M.M. Mestdagh, E.M. Gaigneaux, Catal. Today 112 (2006) 165–168.